Architecture of Succinate Dehydrogenase and Reactive Oxygen Species Generation

Victoria Yankovskaya, *et al.*

Science **299**, 700 (2003);
DOI: 10.1126/science.1079605

between *Drosophila melanogaster* and *Anopheles gambiae*, although the X chromosome of the latter is smaller (*18*). Thus, we can test the idea of preferential loss of male-biased genes from the X chromosome. It is noteworthy that there have been translocations from X chromosome to autosome (and vice versa) in the two lineages, which have allowed us to determine if movement to an autosome "rescues" X-chromosome male-biased genes from loss. When we plotted the ratio of sex-biased expression in *Drosophila* gonads against the probability that a homolog exists in *Anopheles*, two clear correlations were observed. In agreement with traditional comparative studies on limited numbers of genes (*19*), genes highly expressed in males appear to change rapidly. More surprising is the strikingly tight correlation between degree of sex-biased expression and conservation.

Overall, 60% (8513) of the *Drosophila* transcripts represented on the array have homologs in *Anopheles* (*18*). When we tracked changes in linkage between the species, we found that conservation is directly related to sex-biased expression ratios and to chromosomal location. The poorest conservation is between *Drosophila* X-chromosome male-biased genes and the *Anopheles* X chromosome (Fig. 4A). Indeed, none of the X-chromosome genes showing greater than eightfold overexpression in *Drosophila* males are found on the *Anopheles* X chromosome, but this is not restricted to highly male-biased genes. There is a smooth inverse relationship between degree of male-biased expression and conservation. Translocation to an autosome clearly increases the probability of conservation. The only homologs of *Drosophila* genes with highly male-biased expression found on the *Anopheles* X chromosome are autosomal in *Drosophila* (Fig. 4B), and nearly 30% of *Drosophila* X chromosome, male-biased genes are conserved on an *Anopheles* autosome (Fig. 4C). The best-conserved male-biased genes are autosomal in both species (Fig. 4D). Thus, continued X linkage of a gene with male-biased expression in both lineages, presumably reflecting the configuration of the ancestral X chromosome, is highly disfavored. These data unambiguously indicate that X linkage lowers the effective "life-span" of a gene with male-biased expression. Movement to the autosomes can occur by translocation or by preferential retrotransposition of male-biased genes as has been recently shown (*20*).

It has been postulated that the X chromosome is a favored location for evolution of male advantage alleles because of the lack of a less advantageous second allele at that locus in hemizygotes (*3*). Indeed, in mammals it appears that the X chromosome is the favored location for male-biased expression, at least for a few genes expressed in primary spermatocytes (*4*). However, this may be because of compensation, in advance, for the precocious inactivation of those X chromosomes in preparation for meiosis (*20*). It certainly seems clear that the X chromosome is a poor location for male-biased gene expression in *C. elegans*, and in late spermatocytes of *Drosophila* and humans, where X-chromosome inactivation has been implicated (*11*, *12*, *15*, *20*). However, X inactivation does not explain the paucity of X-chromosome genes showing male-biased expression in the *Drosophila* soma, or indeed in the bulk of spermatogenesis.

There are multiple forces shaping the X chromosome. Our data suggest that at least some of them result in demasculinization, because of net selection against extant, or poor net de novo creation of, male-biased genes. Although such antagonistic selection has been proposed as a force for masculinizing the X chromosome, or feminizing a chromosome with restricted passage through females, it is easily adapted to the idea of demasculinization. Because the X chromosome is present in females two-thirds of the time, there is pressure against genes with male-biased expression that are detrimental to females. However, it seems odd that those genes showing the most male-bias, and therefore generally showing the lowest expression in females, would be subjected to the strongest negative selection in females. Is leaky expression of genes directing male development sufficiently detrimental to females to be selected against? How can the X chromosome not be favored for de novo male-biased genes, when hemizygosity means that even normally recessive genes are "dominant" and thus subjected to immediate selection in males? Clearly, the sequencing and expression profiles of more organisms to develop better models of the ancestral X chromosome will greatly aid the unraveling of these and other long-standing questions of sex chromosome origin and divergence.

References and Notes

1. B. S. Baker, M. Gorman, I. Marin, *Annu. Rev. Genet.* **28**, 491 (1994).
2. B. Oliver, *Int. Rev. Cytol.* **219**, 1 (2002).
3. W. R. Rice, *Evolution* **38**, 735 (1984).
4. P. J. Wang, J. R. McCarrey, F. Yang, D. C. Page, *Nature Genet.* **27**, 422 (2001).
5. R. Edgar, M. Domrachev, A. E. Lash, *Nucleic Acids Res.* **30**, 207 (2002).
6. M. N. Arbeitman *et al.*, *Science* **297**, 2270 (2002).
7. W. Jin *et al.*, *Nature Genet.* **29**, 389 (2001).
8. J. Andrews *et al.*, *Genome Res.* **10**, 2030 (2000).
9. W. J. Swanson, A. G. Clark, H. M. Waldrip-Dail, M. F. Wolfner, C. F. Aquadro, *Proc. Natl. Acad. Sci. U.S.A.* **98**, 7375 (2001).
10. G. M. Rubin *et al.*, *Science* **287**, 2222 (2000).
11. Y. Fong, L. Bender, W. Wang, S. Strome, *Science* **296**, 2235 (2002).
12. W. G. Kelly *et al.*, *Development* **129**, 479 (2002).
13. E. Lifschytz, D. L. Lindsley, *Proc. Natl. Acad. Sci. U.S.A.* **69**, 182 (1972).
14. L. Rastelli, M. I. Kuroda, *Mech. Dev.* **71**, 107 (1998).
15. V. Reinke *et al.*, *Mol. Cell* **6**, 605 (2000).
16. M. D. Adams *et al.*, *Science* **287**, 2185 (2000).
17. R. A. Holt *et al.*, *Science* **298**, 129 (2002).
18. E. M. Zdobnov *et al.*, *Science* **298**, 149 (2002).
19. G. J. Wyckoff, W. Wang, C. I. Wu, *Nature* **403**, 304 (2000).
20. E. Betrán, K. Thorton, M. Long, *Genome Res.* **12**, 1854 (2002).

21. We acknowledge discussions and technical assistance from our colleagues, especially C. Chan, J. Dean, M. Doctolero, A. Lash, J. Minor, M. Romiti, M. Vainer, H. Yue, and B. Wang. D.N. was supported in part by NSF DMI-0087032.

Supporting Online Material
www.sciencemag.org/cgi/content/full/1079190/DC1
Materials and Methods
Fig. S1
Table S1
References

8 October 2002; accepted 13 December 2002
Published online 2 January 2003;
10.1126/science.1079190
Include this information when citing this paper.

Architecture of Succinate Dehydrogenase and Reactive Oxygen Species Generation

Victoria Yankovskaya,[1]* Rob Horsefield,[2]* Susanna Törnroth,[3]* César Luna-Chavez,[1,4]† Hideto Miyoshi,[5] Christophe Léger,[6]‡ Bernadette Byrne,[2] Gary Cecchini,[1,4]§ So Iwata[2,3,7]§

The structure of *Escherichia coli* succinate dehydrogenase (SQR), analogous to the mitochondrial respiratory complex II, has been determined, revealing the electron transport pathway from the electron donor, succinate, to the terminal electron acceptor, ubiquinone. It was found that the SQR redox centers are arranged in a manner that aids the prevention of reactive oxygen species (ROS) formation at the flavin adenine dinucleotide. This is likely to be the main reason SQR is expressed during aerobic respiration rather than the related enzyme fumarate reductase, which produces high levels of ROS. Furthermore, symptoms of genetic disorders associated with mitochondrial SQR mutations may be a result of ROS formation resulting from impaired electron transport in the enzyme.

Succinate dehydrogenase (complex II; or succinate:ubiquinone oxidoreductase, SQR) is a functional member of both the Krebs cycle and the aerobic respiratory chain. Complex II couples the oxidation of succinate to fumarate in the mitochondrial matrix (or cytoplasm in bac-

teria) with the reduction of ubiquinone in the membrane (*1*). Mammalian mitochondrial and many bacterial SQRs are composed of two hydrophilic subunits, a flavoprotein (SdhA) and iron-sulfur protein (SdhB) subunit, and two hydrophobic membrane anchor subunits, SdhC and SdhD, which contain one heme *b* and provide the binding site for ubiquinone (*1*).

In eukaryotes, mutations of nuclear-encoded SQR genes can manifest themselves with a wide variety of clinical phenotypes, including optic atrophy, tumor formation, myopathy, and encephalopathy (*2*). Mutations in the SQR genes have been classified into two categories: (i) mutations in SdhA that cause disorders displaying a phenotype resembling other Krebs cycle gene defects, including Leigh syndrome (*3*); and (ii) those in SdhB, SdhC, and SdhD that cause the tumors observed in hereditary paraganglioma and/or pheochromocytoma (*4*, *5*). In *Caenorhabditis elegans*, the *mev-1* mutant, which has a point mutation in the SdhC subunit, is reported to be hypersensitive to oxygen and to develop a premature aging phenotype (*6*, *7*). Although it has been suggested that these disorders can be caused by oxidative stress produced by complex II itself (*2*), no detailed molecular mechanism has been proposed.

Succinate dehydrogenase is closely related to fumarate reductase (menaquinol:fumarate oxidoreductase or QFR), which catalyzes the opposite reaction to that of SQR during anaerobic respiration in bacteria (*8*). SQR and QFR are suggested to have evolved from a common ancestor (*9*), and in *E. coli* they are capable of functionally replacing each other (*10*, *11*). The hydrophilic SdhA and SdhB subunits exhibit strong sequence similarity to their QFR counterparts; however, the sequences of transmembrane subunits are less well conserved. The structures of QFR from both *E. coli* (containing no heme) and *Wolinella succinogenes* (containing two hemes) have been solved to 2.7 and 2.2 Å, respectively (*12*, *13*). Two spatially separated menaquinone-binding sites have been identified in the *E. coli* QFR structure (*12*, *13*), but the quinone-binding site position(s) in the *W. succinogenes* structure has yet to be determined. In many bacteria, including *E. coli*, and in parasites like *Ascaris suum*, SQR is expressed and used under aerobic conditions but QFR is used under anaerobic conditions (*1*, *8*, *14*, *15*). Because both SQR and QFR can catalyze the same reactions in vivo and in vitro, it has been unclear why cells would need to produce SQR under aerobic conditions.

Here, we report the structure of SQR from *E. coli* at 2.6 Å resolution. Details of sample preparation, crystallization, and structure determination are provided in (*16*). Statistics for data collection and structure determination are summarized in Table 1.

The overall structure of SQR is shown in Fig. 1, A and B. SQR is packed as a trimer (total molecular weight 360 kD), with the monomers related by a crystallographic three-fold axis. This distinguishes the SQR structure from the reported QFR structures, which form dimers (*12*). The trimer shows a mushroom- like shape, with the largest dimensions 125 Å along the membrane and 125 Å along the membrane normal. The monomers are very tightly packed, with a contact surface of 1242 Å^2, and this observation suggests that this trimer association is physiological.

Although the structures of the SdhA and SdhB subunits of SQR are similar to those of *E. coli* (*17*) and *W. succinogenes* QFRs (*18*), the transmembrane anchor structures from these three enzymes are considerably different (fig. S1). The SdhA and SdhB subunits (total 826 residues) can be superimposed on the equivalent subunits of *E. coli* and *W. succinogenes* QFR (PDB entries 1KF6 and 1QLA, respectively), with root mean square (r.m.s.) deviations of 1.5 Å for 744 Cα atoms and 1.9 Å for 683 residues, respectively, calculated with program O (*17*). It is impossible, however, to superimpose the transmembrane subunits (SdhC and SdhD) unambiguously onto their counterparts in the QFRs. There are three primary differences in the transmembrane anchors of SQR and QFRs (Fig. 2): (i) Number of subunits. *E. coli* SQR and QFR have two subunits (three transmembrane helices for each), whereas *W. succinogenes* QFR has only one subunit, with five transmembrane helices. (ii) Number of heme *b* molecules. *E. coli* SQR has only one heme *b*; however, *W. succinogenes* QFR has two heme *b* molecules

Table 1. Data collection, refinement, and phasing statistics for the *E. coli* SQR structure determination.

	Data collection and phasing				
Data set	Inflection	Peak	Remote	High resolution	DNP-17 complex
Beam line	ESRF ID29	ESRF ID29	ESRF ID29	SLS X06SA	ESRF ID14/EH2
Wavelength (Å)	1.7416	1.7382	0.9756	1.0081	0.9150
Resolution (Å)	40.0–3.2	40.0–3.2	40.0–3.2	40.0–2.6	40.0–2.9
Total observation	69,082	72,443	75,950	152,468	119,504
Unique reflections	28,173	28,465	29,175	53,727	42,735
Completeness (%)*	88.0 (69.8	89.2 (77.0)	91.4 (86.3)	89.9 (90.0)	98.1 (96.6)
Redundancy	2.5	2.5	2.6	2.9	2.8
R_{sym} (%)*†	9.0 (40.5‡)	7.2 (28.2)	10.1 (44.7‡)	7.6 (40.8‡)	11.6 (42.8‡)
Phasing power§	0.59	0.65	–	–	–

	Refinement‖	
Data set	High resolution	DNP-17 complex
Resolution (Å)*	40.0–2.6 (2.69–2.6)	40.0–2.9 (2.96–2.90)
R factor (%)*¶	24.7 (32.1‡)	27.1 (32.6‡)
R_{free} (%)*#	28.9 (36.8‡)	29.6 (36.5‡)
Average *B* values (Å^2)	45.0	81.4
r.m.s. deviations from ideal values		
Bond length (Å)	0.008	0.009
Bond angles (°)	1.4	1.4
Dihedral angles (°)	21.3	21.2
Improper torsion angles (°)	1.0	1.0
Ramachandran plot (non-Gly, non-Pro residues)		
Most-favored regions (%)	86.6	85.1
Additional allowed regions (%)	12.3	13.2
Generously allowed regions (%)	0.8	1.2
Disallowed regions (%)	0.3	0.4

*Values in parentheses are for the highest-resolution shell. † $R_{sym} = \Sigma_h\Sigma_i|I_i(h) - \langle I(h)\rangle|/\Sigma_h\Sigma_i I(h)$, where $Ii(h)$ is the ith measurement. ‡The last shell R_{merge} for the high-resolution set is rather high as a result of strong anisotropy. However, we include the data for the refinement because the refinement *R*-factor and R_{free} for the shell is reasonably low, which indicates the data in this shell are still useful for the refinement. §Phasing power is the r.m.s. value of F_h divided by the r.m.s. lack-of-closure error. ‖All the observed reflections are used for the refinement. ¶*R*-factor $= \Sigma_h||F(h)_{obs}| - |F(h)_{calc}||/\Sigma_h|F(h)_{obs}$. #$R_{free}$ was calculated for 1% of reflections randomly excluded from the refinement.

[1]Molecular Biology Division, VA Medical Center, San Francisco, CA 94121, USA. [2]Department of Biological Sciences, Imperial College London, London SW7 2AY, UK. [3]Department of Biochemistry, Uppsala University, BMC Box 576, S-75123 Uppsala, Sweden. [4]Department of Biochemistry and Biophysics, University of California, San Francisco, CA 94143, USA. [5]Division of Applied Life Sciences, Graduate School of Agriculture, Kyoto University, Sakyo-ku, Kyoto 606-8502, Japan. [6]Inorganic Chemistry Laboratory, Oxford University, South Parks Road, Oxford OX1 3QR, UK. [7]Division of Biomedical Sciences, Imperial College London, London SW7 2AZ, UK.

*These authors contributed equally to this work.
†Present address: Center for Biophysics and Computational Biology, Department of Biophysics, University of Illinois Urbana-Champaign, Urbana, IL 61801, USA.
‡Present address: BIP07-CNRS, 31, Chemin Joseph Aiguier, 13402 Marseille, France.
§To whom correspondence should be addressed. E-mail: s.iwata@ic.ac.uk or ceccini@itsa.ucsf.edu

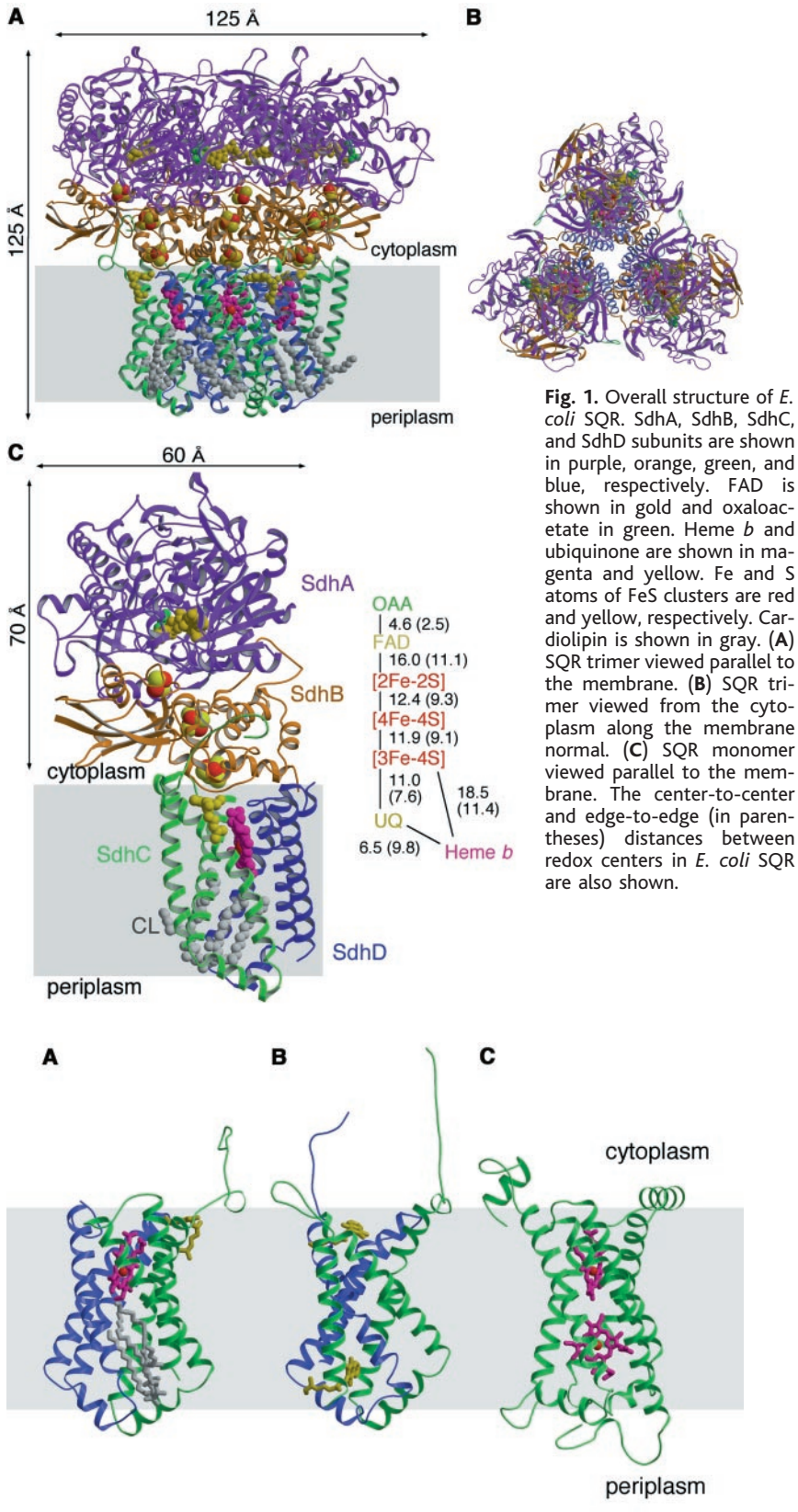

Fig. 1. Overall structure of *E. coli* SQR. SdhA, SdhB, SdhC, and SdhD subunits are shown in purple, orange, green, and blue, respectively. FAD is shown in gold and oxaloacetate in green. Heme *b* and ubiquinone are shown in magenta and yellow. Fe and S atoms of FeS clusters are red and yellow, respectively. Cardiolipin is shown in gray. (**A**) SQR trimer viewed parallel to the membrane. (**B**) SQR trimer viewed from the cytoplasm along the membrane normal. (**C**) SQR monomer viewed parallel to the membrane. The center-to-center and edge-to-edge (in parentheses) distances between redox centers in *E. coli* SQR are also shown.

Fig. 2. Comparison of the transmembrane domain structures of (**A**) *E. coli* SQR, (**B**) *E. coli* QFR (PDB entry 1L0V), and (**C**) *W. succinogenes* QFR (PDB entry 1QLA). All three are viewed parallel to the membrane from the same direction. SdhC and SdhD subunits are shown in green and blue, respectively. The equivalent subunits in *E. coli* QFR are shown in the same colors. *W. succinogenes* QFR has a single transmembrane subunit. Ubiquinone and menaquinone are shown in yellow in (A) and (B). Heme *b* and cardiolipin are shown in pink and gray, respectively. Gray shading represents the position of the membrane.

and *E. coli* QFR has none. The position of heme *b* in *E. coli* SQR is only 1.5 Å away from the position of heme b_P in *W. succinogenes* QFR when the two structures are superimposed by program O (*17*), based on the Cα atom positions in SdhA and SdhB subunits. The position of heme b_D of *W. succinogenes* QFR has been replaced by two acyl groups of cardiolipin in the *E. coli* SQR structure. (iii) Position of the quinone-binding sites. This will be discussed below.

All redox centers and the succinate and quinone-binding sites are clearly assigned in the electron density map (Fig. 1C). The SdhA subunit contains a covalently attached flavin adenine dinucleotide (FAD) cofactor and the substrate-binding site. In the crystal structure, density at the substrate-binding site was assigned as oxaloacetate, an inhibitor of SQR that remains bound during the purification process (*18*). The structure of the substrate-binding site is very similar to those of QFRs. The SdhB subunit contains three iron sulfur clusters: [2Fe-2S], [4Fe-4S], and [3Fe-4S]. Some small but important differences are observed between the SQR and QFR iron sulfur clusters. As predicted by sequence alignments and mutagenesis studies (*19*, *20*), one of the [2Fe-2S] cluster ligands is an Asp (Asp B63) such as those found in some bacterial ferredoxins (*21*), whereas QFRs and most SQRs have a Cys residue. A fifth Cys residue (Cys B154), which is conserved among SQRs but not in QFR, is associated with the [4Fe-4S] cluster. In the structure, Cys B154 forms a hydrogen bond with the thiol group of a [4Fe-4S] ligand Cys B152. These differences could be related to the observed difference in redox potentials between SQR and QFR iron-sulfur clusters (*1*) and could have physiological importance, as discussed below.

The substrate-binding site and ubiquinone-binding site are connected by a chain of redox centers including FAD, [2Fe-2S], [4Fe-4S], and [3Fe-4S] clusters. This chain extends over 40 Å through the enzyme monomer (Fig. 1C). All edge-to-edge distances between the centers are less than the suggested 14 Å limit for physiological electron transfer (*22*). In contrast, the shortest distance between metal centers in adjacent monomers is 30.4 Å (edge-to-edge for heme *b*), which indicates that electron transfer likely occurs within each monomer.

Unexpectedly, heme *b* is not located in this pathway. It seems that the electron transfer pathway is branched at the [3Fe-4S] cluster to ubiquinone and heme *b*. Edge-to-edge distance between the [3Fe-4S] cluster and ubiquinone is 7.6 Å, shorter than the 11.4 Å between the [3Fe-4S] cluster and heme *b*. Additionally, ubiquinone has a higher redox potential (~ +100 mV) than does heme *b* (+36 mV). Although electrons can be transferred either to ubiquinone or to heme *b* from the [3Fe-4S] cluster, transfer to ubiquinone is preferable. Mutants of heme *b* ligands strongly affect the

heme potential but nonetheless permit SQR activity, suggesting that flux through the heme *b* is not essential for quinone reduction (*23*). All known SQR complexes contain at least one heme *b*; however, this is not the case for QFR. Because *E. coli* QFR is stable without a heme *b*, the presence of heme may not be an absolute structural requirement for complex II. The physiological importance of this heme *b* is discussed below.

The SdhC and SdhD subunits form a membrane-bound cytochrome *b* with six transmembrane helices containing one heme *b* group and a ubiquinone-binding site (Fig. 3, A and B). Two well-ordered phospholipid molecules—one cardiolipin (a prevalent lipid in the inner membrane of mitochondria and bacteria) and one phosphatidylethanolamine—were also observed. Two acyl groups of cardiolipin occupy the hydrophobic space below the heme *b*, which accommodates the second heme *b* in the *W. succinogenes* QFR structure.

Electron density assigned as ubiquinone is located in a cleft composed of residues from three subunits, SdhB, SdhC, and SdhD, close to the [3Fe-4S] cluster (Fig. 3, A and B). When the enzyme was co-crystallized with a competitive inhibitor of ubiquinone, 2-(1-methylhexyl)-4,6-dinitrophenol (DNP-17) (*24*), the density for the inhibitor was found at the same position, confirming this site as the physiological quinone-binding site (Fig. 3C). The side chains of Tyr D83 and Trp B164 are direct ligands of the O1 atom of ubiquinone (Fig. 3, C and D). Tyr D83 forms an additional hydrogen bond to Arg C31, which could reduce the pK_a of Tyr D83 side chain; therefore, a proton may directly be translocated from the Tyr D83 to the O1 atom of ubiquinone when it is reduced. The Arg C31 side chain is within 4 Å of a methoxy group of ubiquinone. This seems to be important for the substrate specificity of the ubiquinone-binding site. In the DNP-17 complex structure, Arg C31 recognizes the 6-nitro group of the inhibitor and is likely to be a key residue for substrate and inhibitor specificity. Arg C31 forms a salt bridge to a heme *b* propionate. The ubiquinone-binding site of the *E. coli* SQR is the first example of a tyrosine side chain functioning as a quinone ligand. Many quinone-binding sites reported to date have a His residue hydrogen bonded to the O1 or O4 carbonyl groups (*25*). There is no protein side chain in proximity to the O4 carbonyl oxygen. It is possible that a water molecule is the O4 ligand as observed in the menaquinone-binding site in formate dehydrogenase-N (*26*). The O4 atom is close to the surface and could be directly connected to the cytoplasm by a water chain.

The quinone ring is sandwiched by Ile C28 and Pro B160 (Fig. 3D). These residues, along with Ile B209, Trp B163, Trp B164, and Ser C27 (Cβ atom), form the hydrophobic environment of the quinone-binding pocket. The residues in the quinone-binding site, His B207, Pro B160, Trp B163, Trp B164, Ile B209, Ile C28, Arg C31, Tyr D83, and Asp D82, are strictly conserved among human, mouse, *Paracoccus denitrificans,* and *E. coli* SQRs. Mutation of the residue equivalent to Pro B160 in humans causes hereditary paraganglioma (*27*). Mutation of the residue equivalent to Ile C28 in *C. elegans* (*mev-1*) results in a loss of ubiquinone reductase activity (*6*) and increased ROS production (*7*). These results strongly indicate that mitochondrial SQRs have the same ubiquinone-binding site as *E. coli* SQR.

In contrast, the residues in this region are poorly conserved in QFRs. In *E. coli* QFR, two menaquinone-binding sites, one on the periplasmic side (Q_D site) and the other on the cytoplasmic side (Q_P site), have been determined (*12*). Both menaquinone-binding sites are different from the SQR ubiquinone-binding site; even the Q_P site is about 15 Å away from the SQR ubiquinone-binding site when both enzymes are superimposed by program O (*17*), based on the Cα atom positions in the hydrophilic subunits (*12*). The position equivalent to the Q_P site is occupied by the heme *b* propionate in the SQR structure. For *W. succinogenes* QFR, where the quinone-binding site has yet to be determined, a position equivalent to the SQR ubiquinone-binding site does not exist (*13*). This enzyme has a single integral membrane subunit, and a horizontal helix connecting helices III and IV, making this site totally inaccessible from the outside. These results suggest that the SQR quinone-binding site is different from those of QFRs, which distinguishes SQR from QFR within this family of enzymes.

On the basis of the structure of SQR, the genetic mutations causing hereditary paraganglioma/pheochromocytoma (*2*, *28*) can be classified into (i) nonsense mutations that produce truncated proteins, which fundamentally disrupt the structure of the transmem-

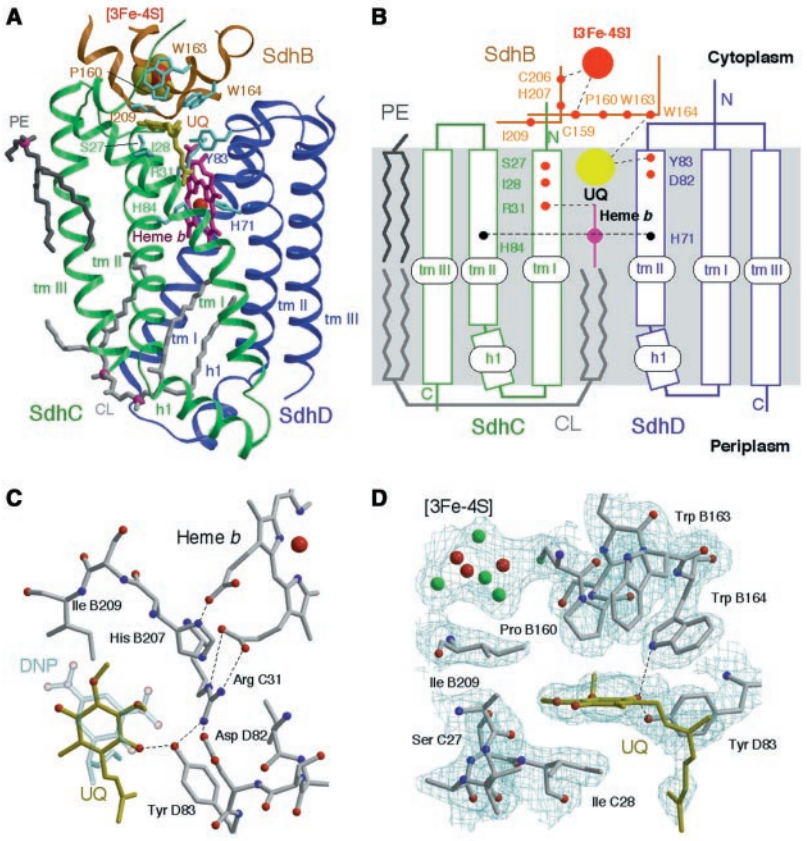

Fig. 3. Structure of the integral membrane subunits. SdhB is only partially shown. (**A**) View parallel to the membrane. Essential residues for ubiquinone-binding and heme *b* ligation are shown in cyan. Transmembrane helices for both SdhC (green) and SdhD (blue) subunits are numbered from tm I to tm III. Ubiquinone (UQ, yellow), heme *b* (magenta), and the [3Fe-4S] cluster are shown. Cardiolipin (CL, light gray) and phosphatidylethanolamine (PE, dark gray) are also shown. (**B**) Secondary structure schematic of (A). The residues involved in heme *b* and ubiquinone (UQ) binding are shown in black and red, respectively. (**C**) Polar interactions in the ubiquinone-binding site. The DNP-17 structure observed in the DNP-17 complex is superimposed onto ubiquinone (UQ). This is a view along the membrane normal from the cytoplasmic side. (**D**) Hydrophobic residues in the ubiquinone-binding site. This is a view parallel to the membrane. A $2|F_{obs}| - |F_{calc}|$ electron density map of the region is also shown. The map was contoured at 1.3 σ.

brane subunits and/or association of the catalytic domain subunits SdhAB to the membrane; (ii) point mutations in the quinone-binding site; and (iii) point mutations around heme *b*. Interestingly, all of these mutations result in the same phenotype, indicating that they all cause the same problem to the cell. In the *C. elegans mev-1* mutant, SQR can oxidize succinate to fumarate but cannot transfer electrons to ubiquinone. The observed increased ROS level is explained by the leakage of electrons, which are released from succinate but not accepted by ubiquinone because of the dysfunctional binding site. It has been suggested that the human genetic disorders that result from mutations of SdhB, SdhC, and SdhD subunits are also induced by ROS formation (*2*).

The detailed mechanism of superoxide formation by the SQR/QFR family has recently been studied (*29*). QFR can function perfectly well as an SQR as far as enzymatic activity is concerned (*1*) and, indeed, *E. coli* can grow aerobically in the complete absence of SQR when QFR is expressed instead (*10*). However, while oxidizing succinate under aerobic conditions, *E. coli* QFR produces hydrogen peroxide (which SQR does not produce) and 25 times as much superoxide as *E. coli* SQR (*29*). It was concluded that ROS is formed primarily at the FAD level because it is suppressed by an excess of substrate or substrate analogs. This is a logical conclusion, because many other flavoenzymes are known to be major sources of ROS.

The key difference between SQR and QFR lies in the arrangement of redox potentials among the redox centers (Table 2). *E. coli* SQR maintains the high redox potential centers ([3Fe-4S] and heme *b*, which would attract electrons) close to the quinone-binding site. In contrast, in *E. coli* QFR, FAD and the [2Fe-2S] cluster have the highest redox potentials. These arrangements are favorable for the respective physiological catalytic reactions (i.e., ubiquinone reduction for SQR and fumarate reduction/menaquinol oxidation for QFR) but are not essential because both enzymes can catalyze the QFR and SQR reactions.

Table 2. Electron distribution among the redox centers of *E. coli* SQR and QFR.

	Redox potentials (mV)		Electron distribution* (number of electrons)		
	SQR	QFR	SQR	SQR (without heme)	QFR
FAD	–79†	–50	0.02	0.18	1.0
[2Fe-2S]	+10	–35	0.43	0.84	0.65
[4Fe-4S]	–175	–310	0.00	0.00	0
[3Fe-4S]	+65	–67	0.87	0.98	0.34
heme *b*	+35	–	0.68	–	–

*The distribution of two electrons was calculated assuming an equilibrium distribution among independent redox centers of given reduction potentials at 298 K. One-electron reduction potentials of the flavin quinone/semiquinone and semiquinone/hydroquinone are treated as the same. For details, see the main text and (*16*). †The value for bovine SQR is used.

To quantify the effect, we calculated the electron distribution among the redox centers (Table 2). For this calculation, we assumed that two electrons have been transferred from succinate to FAD but that the quinone site is not occupied (*16*). Table 2 shows the number of electrons distributed on each of the redox centers of SQR and QFR under this condition. In the case of SQR, electrons are immediately removed from FAD to the [3Fe-4S] cluster and heme *b*, and only 0.02 electrons stay at FAD (i.e., 98% of FAD stays oxidized). However, for QFR, 1.0 electron/FAD is observed; thus, the reactive electron density is 50 times greater at the FAD where electrons are accessible to molecular oxygen because the FAD is directly exposed to the solvent. The situation should be similar during enzymatic catalysis, as intramolecular electron transfer is expected to be faster than turnover (*21*). This evidence strongly suggests that the buildup of electrons around FAD is the cause of high-level ROS production by QFR, as suggested by Messner and Imlay (*29*). This explains why bacteria and parasites use QFR under anaerobic conditions, where it is more efficient for fumarate reduction, and SQR under aerobic conditions, which produces considerably less ROS.

It seems that there has been evolutionary pressure for aerobic organisms to choose SQR over QFR to limit the formation of damaging ROS. A possible reason that all known SQRs conserve one or two hemes, even though heme is not in the direct electron transfer pathway between succinate and ubiquinone, could be to prevent ROS formation. In Table 2, we have calculated the electron distribution among the redox centers for SQR without heme *b*. Without heme, electrons could build up on FAD and, in this case, 0.18 electrons would stay at FAD, which is nine times as high as when heme is present. Thus, heme *b* could serve as an electron sink to prevent electron leakage. However, this electron-sink mechanism is less effective for mitochondrial SQRs because the *b* heme has a lower redox potential (–185 mV) (*30*).

The site itself may also have been designed to prevent ROS formation. The ubiquinone-binding site could be a source of ROS formation, particularly if semiquinone, which is a reaction intermediate, is not stabilized. The Q_P site in *E. coli* QFR does not contain an aromatic ring, which may be because semiquinone is only transiently stabilized in the QFR reaction, and in fact the semiquinone is known to be destabilized in the native enzyme (*31*). On the other hand, it has been known for many years that mammalian SQR stabilizes a semiquinone during the quinone reduction reaction (*32*). One of the reasons that SQR uses a different quinone-binding site from QFR is to incorporate Tyr D83, which could stabilize semiquinone. This tyrosine residue is conserved among all SQRs.

The structure of *E. coli* SQR has given the first clues to the molecular mechanisms of a wide range of genetic disorders caused by mutation of the enzyme. *E. coli* SQR is an ideal model system to study these disorders because of the ease of characterization of enzymatic and structural properties of the mutants.

References and Notes

1. For a review, see G. Cecchini, I. Schröder, R. P. Gunsalus, E. Maklashina, *Biochim. Biophys. Acta* **1553,** 140 (2002).
2. For a review, see P. Rustin, A. Rötig, *Biochim. Biophys. Acta* **1553**, 117 (2002).
3. T. Bourgeron *et al.*, *Nature Genet.* **11,** 144 (1995).
4. B. E. Baysal *et al.*, *Science* **287,** 848 (2000).
5. S. Niemann, U. Müller, *Nature Genet.* **26,** 268 (2000).
6. N. Ishii *et al.*, *Nature* **394,** 694 (1998).
7. N. Senoo-Matsuda *et al.*, *J. Biol. Chem.* **276,** 41553 (2001).
8. A. Kröger, V. Geisler, E. Lemma, F. Theis, R. Lenger, *Arch. Microbiol.* **158,** 311 (1992).
9. For a review, see L. Hederstedt, *Science* **284,** 1941 (1999).
10. J. R. Guest, *J. Gen. Microbiol.* **122,** 171 (1981).
11. E. Maklashina, D. A. Berthold, G. Cecchini, *J. Bacteriol.* **180,** 5989 (1998).
12. T. M. Iverson, C. Luna-Chavez, G. Cecchini, D. C. Rees, *Science* **284,** 1961 (1999).
13. C. R. D. Lancaster, A. Kröger, M. Auer, H. Michel, *Nature* **402,** 377 (1999).
14. K. Kita, H. Hirawake, H. Miyadera, H. Amino, S. Takeo, *Biochim. Biophys. Acta* **1553,** 123 (2002).
15. J. J. Van Hellmond, A. G. M. Tielens, *Biochem. J.* **304,** 321 (1994).
16. Materials and methods are available as supporting material on *Science* Online.
17. T. A. Jones, J. Y. Zou, S. W. Cowan, M. Kjeldgaard, *Acta Crystallogr.* **A47**, 110 (1991).
18. B. A. C. Ackrell, B. Cochran, G. Cecchini, *Arch. Biochem. Biophys.* **268**, 26 (1989).
19. C. Hägerhäll, *Biochim. Biophys. Acta* **1320**, 107 (1997).
20. M. T. Werth *et al.*, *FEBS Lett.* **299**, 1 (1992).
21. W. R. Hagen *et al.*, *J. Biol. Inorg. Chem.* **5**, 527 (2000).
22. C. C. Page, C. C. Moser, X. Chen, P. L. Dutton, *Nature* **402**, 47 (1999).
23. E. Maklashina, R. A. Rothery, J. H. Weiner, G. Cecchini. *J. Biol. Chem.* **276**, 18968 (2001).
24. V. Yankovskaya *et al.*, *J. Biol. Chem.* **271**, 21020 (1996).
25. N. Fisher, P. R. Rich, *J. Mol. Biol.* **296**, 1153 (2000).
26. M. Jormakka, S. Törnroth, B. Byrne, S. Iwata, *Science* **295**, 1863 (2002).
27. D. Astuti *et al.*, *Am. J. Hum. Genet.* **69**, 49 (2001).
28. B. E. Baysal, *J. Med. Genet.* **39**, 617 (2002).
29. K. R. Messner, J. A. Imlay, *J. Biol. Chem.* **277**, 42563 (2002).
30. L. Yu, J.-X. Xu, P. E. Haley, C.-A. Yu, *J. Biol. Chem.* **262**, 1137 (1987).
31. C. Hägerhäll *et al.*, *J. Biol. Chem.* **274**, 26157 (1999).
32. F. J. Ruzicka, H. Beinert, K. L. Schepler, W. R. Dunham, R. H. Sands, *Proc. Natl. Acad. Sci. U.S.A.* **72**, 2886 (1975).

33. Supported by Biotechnology and Biological Sciences Research Council of the UK, Structural Biology Network of Sweden, Syngenta, and the Department of Veterans Affairs and NIH grant GM61606. We thank E. Mitchell and A. Thompson at ESRF, Grenoble, and T. Tomizaki and C. Schulze-Briese at SLS for technical assistance. We also thank J. Abramson and T. Iverson for critically reading the manuscript. The coordinates for the native SQR and the DNP-17 complex are deposited with PDB (entries 1NEK and 1NEN, respectively).

Supporting Online Material

www.sciencemag.org/cgi/content/full/299/5607/700/DC1
Materials and Methods
Fig. S1
References

21 October 2002; accepted 11 December 2002